GSA Data Repository 2017212

Monsoonal upwelling in the western Arabian Sea since the middle-late Miocene

Guangsheng Zhuang[1], Mark Pagani[2], Yi Ge Zhang[3]

[1] *Department of Geology and Geophysics, Louisiana State University, Baton Rouge, LA 70803*

[2] *Department of Geology and Geophysics, Yale University, New Haven, CT 06520*

[3] *Department of Oceanography, Texas A&M University, College Station, TX 77843*

This PDF file includes:

Materials and methods

Supplementary Text

References

Supplementary figure captions

Three supplementary figures

Four supplementary data tables (Tables DR1-4)

Materials and methods

1. Study material and chronology

Studied samples are cored sediments from Ocean Drilling Program (ODP) Sites 722B on the Owen Ridge and 730A off Oman margin in the western Arabian Sea. The section penetrated at Site 722 ranges in age from the early Miocene to Holocene and contains four lithologic units: Unit I with exclusive foraminifer-bearing to foraminifer-nannofossil ooze and nannofossil ooze (Holocene to late Miocene), Unit II of foraminifer-bearing, radiolarian-bearing, diatomaceous, and diatomaceous marly nannofossil chalks (late to middle Miocene), Unit III of white nannofossil chalk (middle Miocene), and Unit IV of turbidite beds of silty clays capped by nannofossil chalks (early to middle Miocene) (Prell et al., 1990). Site 730 is situated on the Oman continental margin. The sediments recovered at Site 730 are subdivided into three lithologic units: Unit I of marly calcareous ooze (Quaternary), Unit II of diatomaceous marly nannofossil ooze and diatomaceous silty clays (late Miocene to middle Miocene), and Unit III of calcareous marly chalks (early-middle Miocene).

Ages of samples were determined by linear interpolation of absolute constraints from paleomagnetic reversals and faunal datums (Prell et al., 1990) and updated to time scales in Gradstein et al. (2004).

2. Lipid extraction and GDGT analysis

Core sediment samples (about 50g) from ODP Sites 722B and 730A were freeze-dried. The total lipid extraction was performed on a Dionex ASE 300 extractor with 2:1 (v/v)

dichloromethane/methanol. Total lipid extracts (TLEs) were concentrated under a stream of purified N_2 and subsequently separated into compound fractions by applying silica-gel chromatography. TLEs were loaded to the ashed Pasteur pipettes which are loaded with approximately 0.5 g deactivated silica gel (70–230 mesh) and were sequentially eluted with 4 ml hexane, 4 ml dichloromethane and 4 ml of methanol to obtain aliphatic, aromatic and polar fractions, respectively. The methanol fraction containing tetraethers was further purified through a column of activated alumina dissolved in dichloromethane/methanol (1:1, v/v), dried under pure N2 stream, dissolved in an azeotrope of hexane/isopropanol (99:1, v/v), filtered through 0.7μm glass microfiber filter, and analyzed on an Agilent 1200 series high performance liquid chromatography coupled with an Agilent 6130 atmospheric pressure chemical ionization – mass spectrometer following the methodology of Hopmans et al. (2000).

Quantification of GDGTs was based on peak intensities of the [M+H]+ ion. Relative abundances of GDGTs were used to calculate the TEX_{86} index and then converted to SSTs by applying a Bayesian, spatially-varying calibration model (Tables DR1-DR2) (Tierney and Tingley, 2014). The reciprocal calibration (Liu et al., 2009), linear (Kim et al., 2008) and logarithmic models (Kim et al., 2010) were also applied (Tables DR3 and DR4). Repeated measurements of an in-house laboratory standard indicate that analytical precision was ±0.01 TEX_{86} unit.

The ketone fraction was analyzed on a Thermo Trace 2000 gas chromatography equipped with a Restek column (60m × 0.25mm × 0.25μm), a Programmable Temperature

Vaporization (PTV) injector and a Flame Ionization Detector (FID). Relative abundances of C37:3 and C37:2 alkenones were used to compute and subsequently converted to SSTs using the surface sediment linear calibration of Conte et al. (2006). Analytical precision, determined through multiple measurements of an in-house alkenone standard, was ±0.05 unit.

Supplementary Text

1. Climatology

Winds and SSTs: climatology data for wind directions and speeds for July are based on the NCEP-NCAR reanalysis between 1981 and 2016 (Kistler et al., 2001) (Fig. DR1). Sea Surface Temperature (SST) values for July are derived from 1982-2008 (Casey et al., 2010) (Fig. DR1). The wind vectors and SSTs show strong southwest winds during peak South Asian monsoon and upwelling related cooling in the western Arabian Sea.

2. Surface uplift history of Tibetan Plateau

Geological studies, including paleoaltimetry, thermochronology, and structure geology, support an Eocene proto-plateau in the central Tibetan Plateau and the outward expansion during the middle-late Miocene. Constraints on the paleoelevation across the Tibetan Plateau support that the Tibetan Plateau had obtained the present-day dimensions between 16-8 Ma (Fig. DR1).

Paleoaltimetry: Paleoaltimetry studies in the Nima Basin (nm), Lunpola Basin (lp), Linzhou Basin (lz) and Qiangtang (qt) in the south-central Tibetan Plateau and in the

Liming Basin (lm) in the northwestern part of Southeast Tibetan Plateau suggest that high elevations comparable to the present-day elevations have been obtained in the Eocene-Oligocene (DeCelles et al., 2007; Ding et al., 2014; Hoke et al., 2014; Li et al., 2015; Rowley and Currie, 2006; Xu et al., 2013). High elevations were obtained in the Namling Basin (nl) in the Southern Tibetan Plateau no later than 15 Ma (Currie et al., 2005; Spicer et al., 2003), in Zhada Basin (zd), Thakkhola (th), and Gyirong (gy) in Himalayas no later than 9-11 Ma (Ding et al., 2017; Garzione et al., 2000; Rowley et al., 2001; Saylor et al., 2009), and in the Hoh Xil Basin (hx), Qaidam Basin (qd), and Songpan Basin (sp) in the north-central, northern, and eastern Tibetan Plateau between 15 Ma and 10 Ma (Cyr et al., 2005; Polissar et al., 2009; Xu et al., 2016; Zhuang et al., 2014).

Thermochronology & Structure Geology: the collision-related rapid exhumation of basement rocks in the Pamir and western portion of Tibetan Plateau have started in the late Oligocene, experienced intense and rapid rates in the middle-late Miocene (e.g. Cao et al., 2013; Sobel and Dumitru, 1997). The slip motion on the Karakoram initiated in the Miocene (e.g. Robinson, 2009). They support the expansion of Tibetan Plateau towards west in the middle-late Miocene.

3. Iranian Plateau

Faunal fossil, sedimentation and thermochronology studies support that the Tethys Seaway was closed during the middle-late Miocene (Fig. DR1) between the Arabian Peninsular and the Eurasia in Iran. The closure of the Tethys Seaway is aligned with a) the cessation of marine sedimentation in the middle Miocene in Iran (Reuter et al., 2009),

b) the post-early Miocene divergence in faunas in the Mediterranean Tethys, Iran, and Indopacific (e.g. Schuster and Wielandt, 1999), and c) the rapid uplift/exhumation of Zagros Mountains in the Iranian Plateau between 16 and 10 Ma (Ballato et al., 2016).

4. Sea Surface Temperature (SST) reconstruction and evaluation

We applied TEX_{86} and $U^{K'}_{37}$ paleothermometers to core sediment samples (Tables DR1-4). Our new SSTs based on TEX_{86} and $U^{k'}_{37}$ proxies show high consistency with previous study between 10-6 Ma (Fig. DR2). The new SSTs based on the $U^{K'}_{37}$ thermometry maintain values of 27.0-28.2 °C between 15-10 Ma, lower than the TEX_{86}-based SSTs (Fig. DR2; Tables DR3 and DR4). Especially, reconstructed pre-11 Ma TEX_{86}-based SSTs are higher than 29.0 °C, beyond the calibration limit of $U^{K'}_{37}$ thermometry. Therefore, we focus our discussions on TEX_{86}-based SSTs for the period between 15-10 Ma.

TEX_{86}-based SST calibration: We converted TEX_{86} to SSTs by applying a Bayesian, spatially-varying calibration model (Tables DR1 and DR2) (Tierney and Tingley, 2014). We include 90% confidence level (Fig. DR3). We also applied the reciprocal calibration model (Liu09) of TEX_{86} thermometry proposed by Liu et al. (2009) to calculate sea surface temperatures (SST). The reciprocal model calibrated SSTs show consistency with $U^{K'}_{37}$-based SSTs between 10 Ma and 6 Ma (Tables DR3 and DR4). TEX_{86} linear and logarithmic calibration models (Kim et al., 2008; Kim et al., 2010) gave higher SSTs in comparison to the reciprocal calibration model (Tables DR3 and DR4). The SSTs for all

137 calibration models show similar trend and amplitudes of change in SSTs, confirming our
138 finding of the major drop in SST between 11 Ma and 10 Ma (Fig. DR2).
139
140 Terrestrial inputs of GDGTs, especially from soils, might cause significant bias for
141 TEX_{86}-based SSTs. The relative abundance of branched relative to isoprenoid tetraethers
142 (BIT index) can be used to evaluate the terrestrial inputs of GDGTs. BIT values higher
143 than 0.4 suggest high terrestrial GDGT input. Our BIT values for analyzed samples are
144 extremely low (< 0.1) (Tables DR3 and DR4), indicating negligible terrestrial inputs of
145 GDGTs.
146
147 The weighted average of cyclopentane moieties of GDGTs, also called the Ring Index
148 (RI), has been used to determine if TEX_{86}-based SSTs are influenced by non-thermal
149 factors by evaluating the difference of observed RI values with respect to the theoretical
150 RI values based on published dataset of RI values and TEX_{86} indices from global core-
151 top and mesocosm culture studies (Zhang et al., 2015). If the ΔR is larger than 0.3, that
152 indicates non-thermal factors, like the growth phase and nutrient levels are significant.
153 We applied the RI calculations to our TEX_{86}-based SSTs; almost all calculated ΔR values
154 are less than 0.2 (Tables DR 3 and DR4), supporting that our reconstructed TEX_{86}-based
155 SSTs are reliable.
156
157 The Methane Index (MI) is an useful tool to differentiate between normal marine and
158 hydrate-impacted environments (Zhang et al., 2011). The MI values can range between 0
159 and 1 with values < 0.3-0.5 indicating normal marine environment. All our analyzed

160 samples (except one) have MI values between 0.1-0.3, implying normal marine
161 environments of our studied sediments without influence and biases related to marine gas
162 hydrates.

163 **Cited references**

164 Ballato, P., Cifelli, F., Heidarzadeh, G., Ghassemi, M. R., Wickert, A. D., Hassanzadeh,
165 J., Dupont‐Nivet, G., Balling, P., Sudo, M., and Zeilinger, G., 2016, Tectono‐
166 sedimentary evolution of the northern Iranian Plateau: insights from middle‐late
167 Miocene foreland‐basin deposits: Basin Research, p. 1–30,
168 doi:10.1111/bre.12180.

169 Casey, K. S., Brandon, T. B., Cornillon, P., and Evans, R., 2010, The past, present, and
170 future of the AVHRR Pathfinder SST program, in Oceanography from Space:
171 Revisited, eds. V. Barale, J.F.R. Gower, and L. Alberotanza, Springer, p. 273-287,
172 doi:10.1007/978-90-8681-5_16.

173 Conte, M. H., Sicre, M. A., Rühlemann, C., Weber, J. C., Schulte, S., Schulz‐Bull, D.,
174 and Blanz, T., 2006, Global temperature calibration of the alkenone unsaturation
175 index (UK'_{37}) in surface waters and comparison with surface sediments:
176 Geochemistry, Geophysics, Geosystems, v. 7, Q02005, p. 1–22,
177 doi:10.1029/2005GC001054.

178 Currie, B., Rowley, D., and Tabor, N., 2005, Middle Miocene paleoaltimetry of southern
179 Tibet: Implications for the role of mantle thickening and delamination in the
180 Himalayan orogen: Geology, v. 33, no. 3, p. 181-184, doi: 10.1130/G21170.1.

181 Cyr, A. J., Currie, B. S., and Rowley, D. B., 2005, Geochemical evaluation of
182 Fenghuoshan Group lacustrine carbonates, north-central Tibet: Implications for

183 the paleoaltimetry of the Eocene Tibetan Plateau: Journal of Geology, v. 113, no.
184 5, p. 517-533.
185 DeCelles, P., Quade, J., Kapp, P., Fan, M., Dettman, D., and Ding, L., 2007, High and
186 dry in central Tibet during the Late Oligocene: Earth and Planetary Science
187 Letters, v. 253, p. 389-401.
188 Ding, L., Spicer, R., Yang, J., Xu, Q., Cai, Q., Li, S., Lai, Q., Wang, H., Spicer, T., and
189 Yue, Y., 2017, Quantifying the rise of the Himalaya orogen and implications for
190 the South Asian monsoon: Geology, doi:10.1130/G38583.1.
191 Ding, L., Xu, Q., Yue, Y., Wang, H., Cai, F., and Li, S., 2014, The Andean-type
192 Gangdese Mountains: Paleoelevation record from the Paleocene–Eocene Linzhou
193 Basin: Earth and Planetary Science Letters, v. 392, p. 250-264.
194 Garzione, C. N., Dettman, D. L., Quade, J., DeCelles, P. G., and Butler, R. F., 2000, High
195 times on the Tibetan Plateau: Paleoelevation of the Thakkhola graben, Nepal:
196 Geology, v. 28, no. 4, p. 339-342.
197 Gradstein, F. M., Ogg, J. G., Smith, A. G., Bleeker, W., and Lourens, L. J., 2004, A new
198 geologic time scale, with special reference to Precambrian and Neogene:
199 Episodes, v. 27, no. 2, p. 83-100.
200 Hoke, G. D., Liu-Zeng, J., Hren, M. T., Wissink, G. K., and Garzione, C. N., 2014, Stable
201 isotopes reveal high southeast Tibetan Plateau margin since the Paleogene: Earth
202 and Planetary Science Letters, v. 394, p. 270-278.
203 Hopmans, E. C., Schouten, S., Pancost, R. D., van der Meer, M. T., and Sinninghe
204 Damsté, J. S., 2000, Analysis of intact tetraether lipids in archaeal cell material
205 and sediments by high performance liquid chromatography/atmospheric pressure

chemical ionization mass spectrometry: Rapid Communications in Mass Spectrometry, v. 14, no. 7, p. 585-589.

Kim, J.-H., Schouten, S., Hopmans, E. C., Donner, B., and Damsté, J. S. S., 2008, Global sediment core-top calibration of the TEX 86 paleothermometer in the ocean: Geochimica et Cosmochimica Acta, v. 72, no. 4, p. 1154-1173.

Kim, J. H., Van der Meer, J., Schouten, S., Helmke, P., Willmott, V., Sangiorgi, F., Koç, N., Hopmans, E. C., and Damsté, J. S. S., 2010, New indices and calibrations derived from the distribution of crenarchaeal isoprenoid tetraether lipids: Implications for past sea surface temperature reconstructions: Geochimica et Cosmochimica Acta, v. 74, no. 16, p. 4639-4654.

Kistler, R., Collins, W., Saha, S., White, G., Woollen, J., Kalnay, E., Chelliah, M., Ebisuzaki, W., Kanamitsu, M., and Kousky, V., 2001, The NCEP-NCAR 50-year reanalysis: Monthly means CD-ROM and documentation: Bulletin of the American Meteorological society, v. 82, no. 2, p. 247-267.

Li, S., Currie, B. S., Rowley, D. B., and Ingalls, M., 2015, Cenozoic paleoaltimetry of the SE margin of the Tibetan Plateau: Constraints on the tectonic evolution of the region: Earth and Planetary Science Letters, v. 432, p. 415-424.

Liu, Z., Pagani, M., Zinniker, D., DeConto, R., Huber, M., Brinkhuis, H., Shah, S. R., Leckie, R. M., and Pearson, A., 2009, Global cooling during the Eocene-Oligocene climate transition: Science, v. 323, no. 5918, p. 1187-1190.

Polissar, P. J., Freeman, K. H., Rowley, D. B., McInerney, F. A., and Currie, B. S., 2009, Paleoaltimetry of the Tibetan Plateau from D/H ratios of lipid biomarkers: Earth and Planetary Science Letters, v. 287, no. 1, p. 64-76.

229 Prell, W.L., Niitsuma, N., and Emeis, K., 1990, Oman Margin/Neogene Package, *in* Prell,
230 W.L., et al., Proceedings of the Ocean Drilling Program, Scientific Results, 117:
231 College Station, Texas (Ocean Drilling Program), 638 p.
232 Reuter, M., Piller, W., Harzhauser, M., Mandic, O., Berning, B., Rögl, F., Kroh, A.,
233 Aubry, M.-P., Wielandt-Schuster, U., and Hamedani, A., 2009, The Oligo-
234 /Miocene Qom Formation (Iran): evidence for an early Burdigalian restriction of
235 the Tethyan Seaway and closure of its Iranian gateways: International Journal of
236 Earth Sciences, v. 98, no. 3, p. 627-650.
237 Rowley, D. B., and Currie, B. S., 2006, Palaeo-altimetry of the late Eocene to Miocene
238 Lunpola basin, central Tibet: Nature, v. 439, no. 7077, p. 677-681.
239 Rowley, D. B., Pierrehumbert, R. T., and Currie, B. S., 2001, A new approach to stable
240 isotope-based paleoaltimetry: implications for paleoaltimetry and
241 paleohypsometry of the High Himalaya since the Late Miocene: Earth and
242 Planetary Science Letters, v. 188, no. 1, p. 253-268.
243 Saylor, J., Quade, J., Dettman, D., DeCelles, P., Kapp, P., and Ding, L., 2009, The late
244 Miocene through present paleoelevation history of southwestern Tibet: American
245 Journal of Science, v. 309, no. 1, p. 1-42.
246 Schuster, F., and Wielandt, U., 1999, Oligocene and Early Miocene coral faunas from
247 Iran: palaeoecology and palaeobiogeography: International Journal of Earth
248 Sciences, v. 88, no. 3, p. 571-581.
249 Spicer, R. A., Harris, N. B. W., Widdowson, M., Herman, A. B., Guo, S., Valdes, P. J.,
250 Wolfe, J. A., and Kelley, S. P., 2003, Constant elevation of southern Tibet over
251 the past 15 million years: Nature, v. 421, no. 6923, p. 622-624.

252 Tierney, J. E., and Tingley, M. P., 2014, A Bayesian, spatially-varying calibration model
253 for the TEX 86 proxy: Geochimica et Cosmochimica Acta, v. 127, p. 83-106.
254 Xu, Q., Ding, L., Zhang, L., Cai, F., Lai, Q., Yang, D., and Liu-Zeng, J., 2013, Paleogene
255 high elevations in the Qiangtang Terrane, central Tibetan Plateau: Earth and
256 Planetary Science Letters, v. 362, p. 31-42.
257 Xu, Q., Liu, X., and Ding, L., 2016, Miocene high‐elevation landscape of the eastern
258 Tibetan Plateau: Geochemistry, Geophysics, Geosystems, v. 17, no. 10, p. 4254-
259 4267.
260 Zhang, Y. G., Pagani, M., and Wang, Z., 2015, Ring Index: A new strategy to evaluate
261 the integrity of TEX86 paleothermometry: Paleoceanography, v. 31, p. 220-232.
262 Zhang, Y. G., Zhang, C. L., Liu, X.-L., Li, L., Hinrichs, K.-U., and Noakes, J. E., 2011,
263 Methane Index: a tetraether archaeal lipid biomarker indicator for detecting the
264 instability of marine gas hydrates: Earth and Planetary Science Letters, v. 307, no.
265 3, p. 525-534.
266 Zhuang, G., Brandon, M. T., Pagani, M., and Krishnan, S., 2014, Leaf wax stable
267 isotopes from Northern Tibetan Plateau: Implications for uplift and climate since
268 15 Ma: Earth and Planetary Science Letters, v. 390, p. 186-198.
269
270 FIGURE CAPTIONS
271 Figure DR1. Himalaya-Tibetan Plateau and surrounding regions, showing locations of
272 geology studies and July winds (blue arrows) and sea surface temperature (SST) contours
273 in the northern Indian Ocean. Green circles indicate Ocean Drilling Program (ODP) Sites
274 730A of Oman Margin and 722B and 731A at Owen Ridge. Hexagons denote

paleoaltimetry studies (numbers denoting the minimum timing of high topography). Yellow triangles indicate themochronology studies, revealing the rapid uplift in the Pamir and Iranian Plateau in the middle-late Miocene. Yellow squares are faunal and sedimentary studies that support the closure of the Tethys Seaway in the middle Miocene. See text for detailed information and cited references.

Figure DR2. Sea surface temperature records in the western Arabian Sea. $U^{K'}_{37}$-based SSTs between 11-0 Ma at Site 722B are from Huang et al. (2007). Our new records include $U^{K'}_{37}$-based SSTs and TEX_{86}-based SSTs between 15-6 Ma. Our new SSTs between 10-6 Ma are consistent with previous records; new $U^{K'}_{37}$-based SSTs are divergent from new TEX_{86}-based SSTs between 15-10 Ma.

Figure DR3. **(A)** TEX_{86}-based SSTs with 90% confidence level at ODP Site 722B. **(B)** TEX_{86}-based SSTs with 90% confidence level at ODP Site 730A.

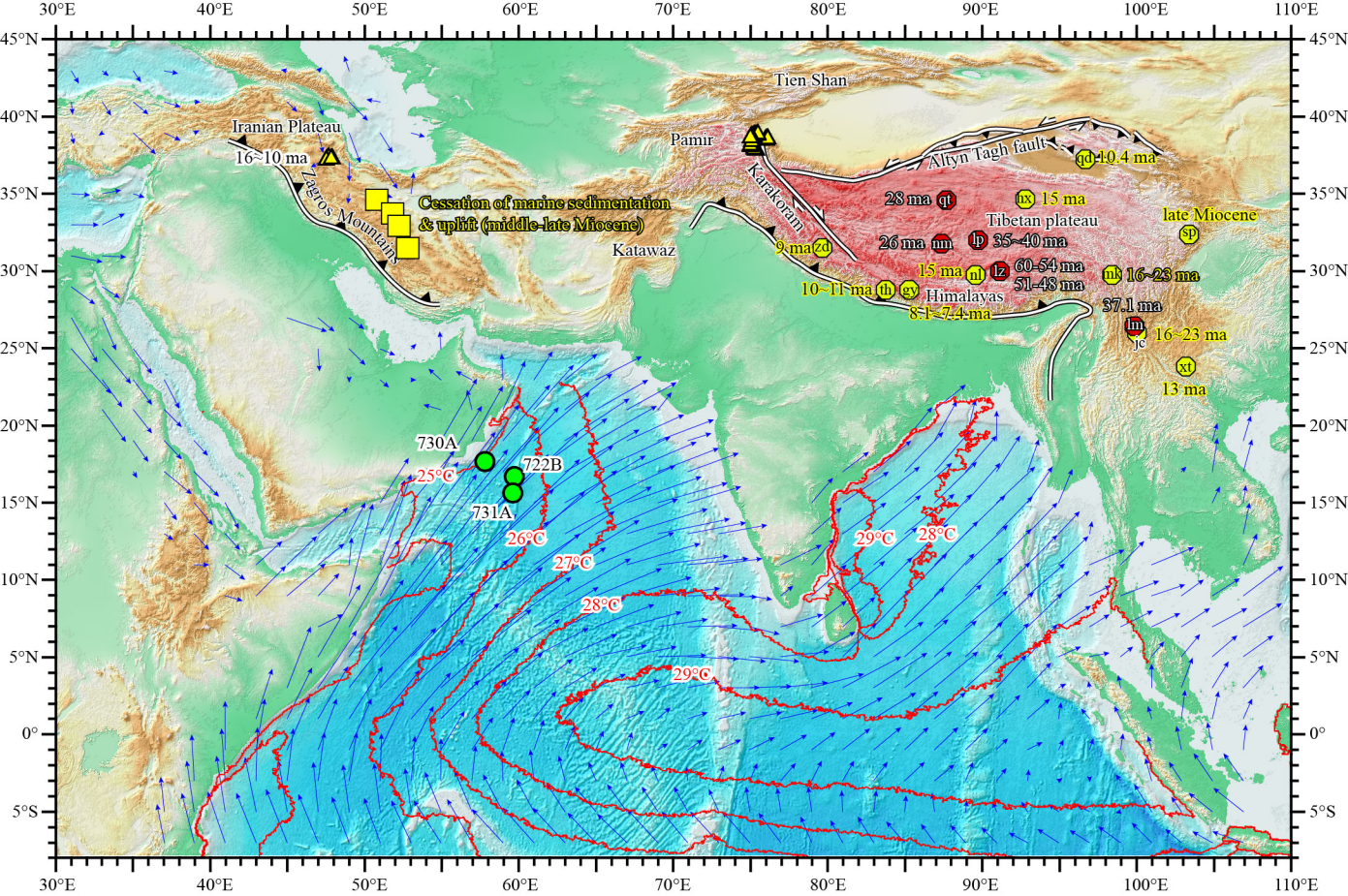
30°E
40°E
50°E
60°E
70°E
80°E
90°E
100°E
110°E
45°N
40°N
35°N
30°N
25°N
20°N
15°N
10°N
5°N
0°
5°S
Tien Shan
Iranian Plateau
16~10 ma
Zagros Mountains
Cessation of marine sedimentation
& uplift (middle-late Miocene)
Pamir
Karakoram
Altyn Tagh fault
qd 10.4 ma
28 ma qt
ux 15 ma
Tibetan plateau
late Miocene
sp
26 ma nm
lp 35~40 ma
Katawaz
9 ma zd
15 ma nj
lz 60-54 ma
51-48 ma
mk 16~23 ma
10~11 ma th
gy Himalayas
8.1~7.4 ma
37.1 ma
lm
jc 16~23 ma
xt
13 ma
730A
722B
731A
25°C
26°C
27°C
28°C
29°C
29°C
28°C

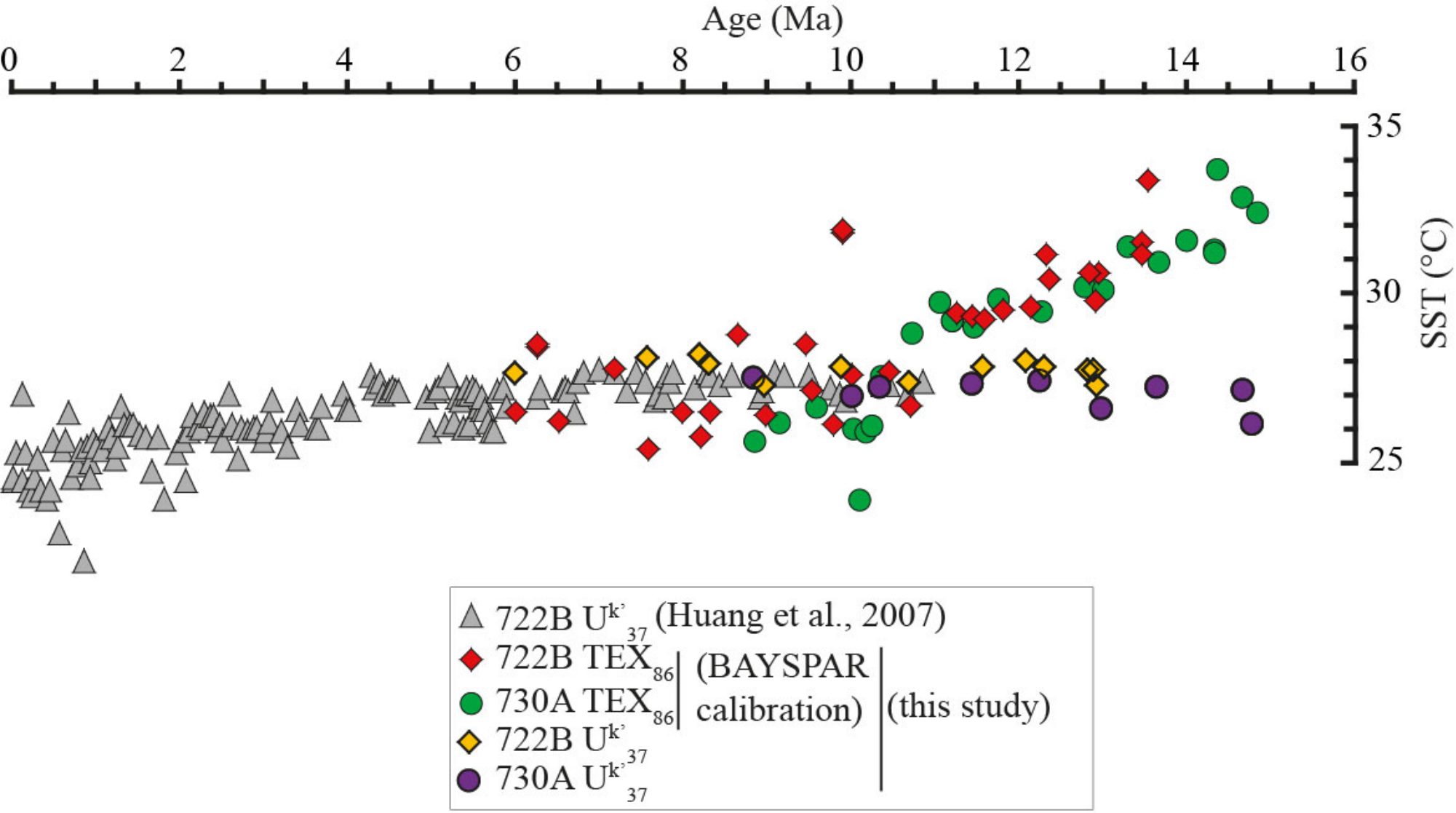
Age (Ma)
0
2
4
6
8
10
12
14
16
35
30
25
SST (°C)
722B U^k'37 (Huang et al., 2007)
722B TEX86
730A TEX86
(BAYSPAR calibration)
722B U^k'37
730A U^k'37
37
(this study)

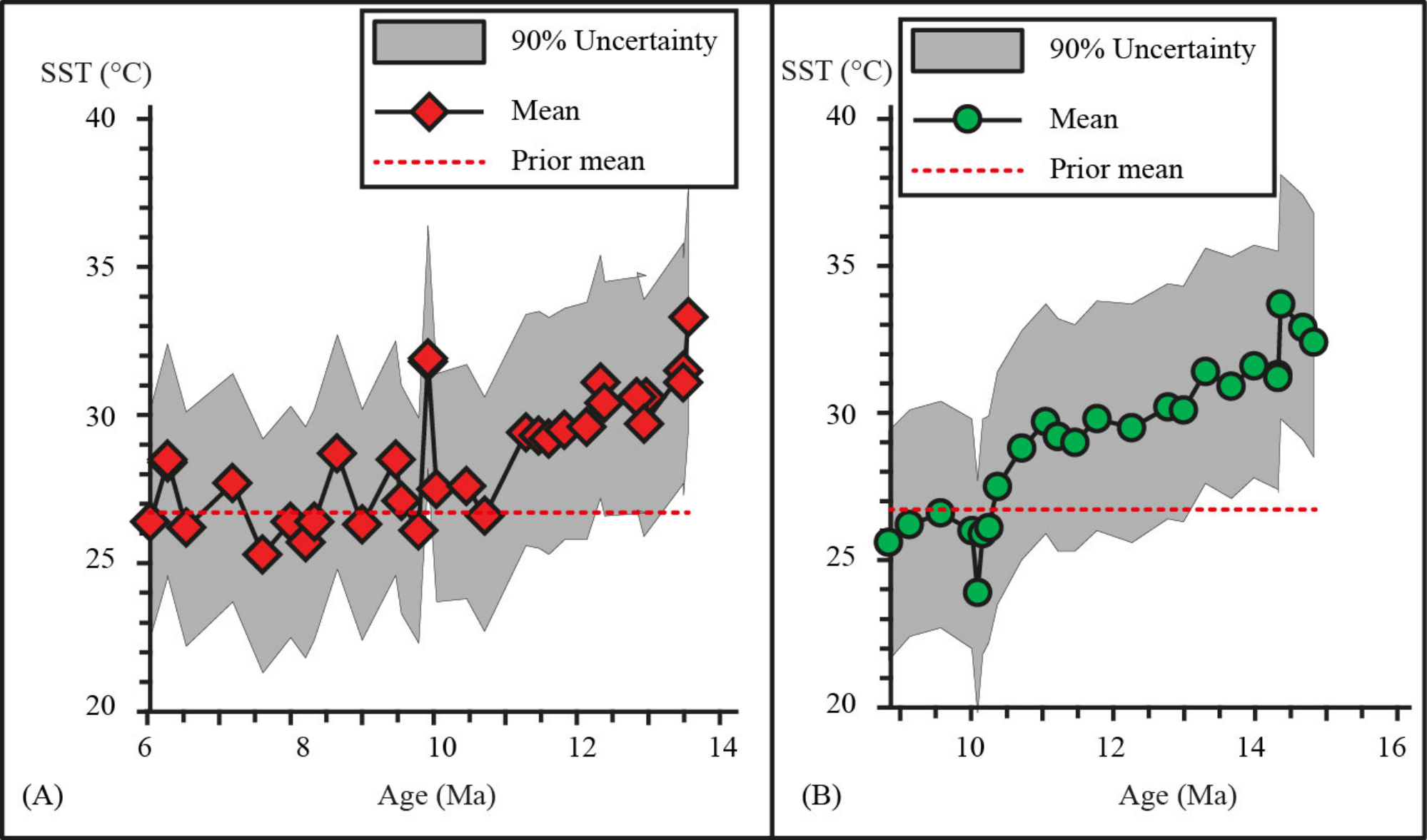
90% Uncertainty
Mean
Prior mean
SST (°C)
40
35
30
25
20
6
8
10
12
14
(A)
Age (Ma)
90% Uncertainty
Mean
Prior mean
SST (°C)
40
35
30
25
20
10
12
14
16
(B)
Age (Ma)

Table DR1. TEX_{86}-SSTs at ODP Site 722B converted by applying a Bayesian, spatially-varying calibration model.

Age	TEX86	SST (°C)		
Ma		5th	50th	95th
6.04	0.71	22.5	26.4	30.2
6.28	0.75	24.5	28.4	32.4
6.28	0.75	24.6	28.5	32.4
6.54	0.71	22.2	26.2	30.1
7.19	0.73	23.7	27.7	31.4
7.61	0.69	21.3	25.3	29.2
8.00	0.71	22.5	26.4	30.3
8.21	0.70	21.8	25.7	29.6
8.33	0.71	22.4	26.4	30.2
8.65	0.75	24.8	28.7	32.7
9.00	0.71	22.4	26.3	30.2
9.47	0.75	24.6	28.5	32.5
9.55	0.72	23.3	27.1	31
9.79	0.71	22.3	26.1	29.9
9.92	0.81	27.9	31.8	36.2
9.92	0.81	28.2	31.9	36.4
10.04	0.73	23.7	27.5	31.4
10.46	0.73	23.8	27.6	31.7
10.71	0.72	22.7	26.6	30.6
11.29	0.77	25.6	29.4	33.4
11.47	0.77	25.5	29.3	33.5
11.61	0.76	25.3	29.2	33.3
11.83	0.77	25.8	29.5	33.6
12.14	0.77	25.8	29.6	33.8
12.33	0.80	27.2	31.1	35.4
12.39	0.79	26.6	30.4	34.5
12.97	0.79	26.7	30.6	34.7
12.84	0.79	26.8	30.6	34.8
12.94	0.77	25.9	29.7	33.9
13.49	0.81	27.7	31.5	35.8
13.49	0.80	27.3	31.1	35.3
13.56	0.84	29.5	33.3	37.7

Table DR2. TEX_{86}-SSTs at ODP Site 730A converted by applying a Bayesian, spatially-varying calibration model.

Age	TEX86	SST (°C)		
Ma		5th	50th	95th
8.84	0.70	21.6	25.6	29.4
9.13	0.71	22.4	26.2	30.1
9.57	0.71	22.7	26.6	30.4
10.01	0.70	22.0	26.0	29.8
10.09	0.66	19.8	23.9	27.7
10.16	0.70	21.8	25.9	29.8
10.25	0.70	22.2	26.1	29.9
10.37	0.73	23.5	27.5	31.4
10.71	0.75	25.0	28.8	32.8
11.05	0.77	25.9	29.7	33.7
11.22	0.76	25.3	29.2	33.2
11.22	0.76	25.3	29.2	33.2
11.46	0.76	25.3	29.0	33.0
11.77	0.77	26.0	29.8	33.8
12.26	0.77	25.6	29.5	33.7
12.77	0.78	26.4	30.2	34.4
12.99	0.78	26.3	30.1	34.3
13.30	0.80	27.6	31.4	35.6
13.66	0.80	27.1	30.9	35.3
13.98	0.81	27.8	31.6	35.7
14.32	0.80	27.4	31.3	35.5
14.32	0.80	27.3	31.2	35.5
14.36	0.85	29.8	33.7	38.1
14.67	0.83	29.1	32.9	37.4
14.82	0.82	28.5	32.4	36.8

Table DR3. Sample information and TEX_{86}-SSTs and $U^{K'}_{37}$-SSTs at ODP Site 722B for the middle-late Miocene.

SAMPLE ID	Depth (mbsf)	AGE (Ma)	MI	RI	RI'	ΔR	BIT	Uk'37	SST	TEX86	Kim08	Liu09	Kim10		
			Zhang09	Zhang16					Conte06				Liu09-revised	TEX86L	TEX86H
722B-24X-2	219.664	6.04	0.19	2.69	2.72	0.03	0.05			0.711	29.1	27.5	27.6	26.1	28.5
722B-24X-6	225.529	6.28	0.20	2.83	2.87	0.04	0.03	0.97	27.7	0.748	31.2	28.6	29.0	28.0	30.0
722B-24X-6-re	225.529	6.28	0.20	2.84	2.88	0.03				0.749	31.3	28.7	29.0	28.2	30.0
722B-25X-4	231.628	6.54	0.19	2.69	2.70	0.02	0.02			0.706	28.9	27.4	27.5	24.9	28.3
722B-27X-1	247.030	7.19	0.18	2.75	2.81	0.06	0.04			0.734	30.4	28.2	28.5	27.3	29.4
722B-28X-1	257.025	7.61	0.22	2.51	2.64	0.13	0.03	0.99	28.1	0.690	28.0	26.8	26.8	25.1	27.6
722B-29X-1	266.123	8.00	0.19	2.68	2.72	0.04	0.04			0.711	29.1	27.5	27.6	25.6	28.5
722B-29X-4	271.620	8.21	0.21	2.54	2.67	0.13	0.03	0.99	28.2	0.698	28.4	27.1	27.1	25.5	27.9
722B-30X-1	276.795	8.33	0.20	2.62	2.72	0.10	0.05	0.98	27.9	0.711	29.2	27.5	27.6	25.9	28.5
722B-31X-5	291.993	8.65	0.18	2.64	2.90	0.25	0.04			0.754	31.6	28.8	29.2	28.9	30.2
722B-33X-3	308.365	9.00	0.19	2.60	2.72	0.11	0.05	0.96	27.2	0.710	29.1	27.5	27.6	25.0	28.4
722B-34X-3	318.083	9.47	0.17	2.68	2.88	0.19	0.06			0.749	31.3	28.7	29.0	28.0	30.0
722B-34X-CC	319.685	9.55	0.18	2.66	2.77	0.12	0.07			0.724	29.9	27.9	28.1	26.4	29.0
722B-35X-1	324.550	9.79	0.19	2.61	2.70	0.09	0.04			0.705	28.8	27.3	27.4	26.4	28.2
722B-35X-3	327.200	9.92	0.13	3.18	3.15	-0.03		0.98	27.8	0.812	34.8	30.4	31.0	29.0	32.4
722B-35X-3-re	327.200	9.92	0.12	3.21	3.16	-0.05				0.814	35.0	30.4	31.0	28.2	32.5
722B-35X-4	329.424	10.04	0.19	*2.49*	*2.81*	*0.32*	0.18			0.733	30.4	28.2	28.5	27.3	29.4
722B-36X-2	335.363	10.46	0.18	2.66	2.81	0.15	0.06			0.734	30.4	28.2	28.5	27.4	29.4
722B-36X-3	337.925	10.71	0.20	2.61	2.74	0.13		0.96	27.4	0.715	29.4	27.6	27.8	26.5	28.6
722B-37X-1	343.747	11.29	0.17	2.83	2.95	0.12	0.06			0.766	32.2	29.1	29.6	29.2	30.7
722B-37X-3	347.103	11.47	0.17	2.82	2.96	0.14	0.05			0.768	32.4	29.2	29.6	29.2	30.8
722B-37X-5	349.898	11.61	0.18	2.78	2.93	0.15		0.98	27.8	0.763	32.1	29.1	29.5	28.3	30.6
722B-38X-1	353.973	11.83	0.18	2.87	2.96	0.10	0.04			0.770	32.5	29.3	29.7	29.0	30.8
722B-38X-5	359.995	12.14	0.17	2.89	2.97	0.08		0.98	28.0	0.771	32.5	29.3	29.7	27.0	30.9
722B-39X-1	363.775	12.33	0.18	2.93	3.09	0.17		0.98	27.9	0.799	34.1	30.0	30.6	30.6	31.9
722B-39X-2	364.853	12.39	0.18	2.89	3.03	0.14	0.05			0.785	33.3	29.7	30.2	29.6	31.4
722B-40-CC	373.665	12.97	0.21	2.86	3.04	0.18		0.96	27.3	0.788	33.5	29.8	30.3	30.8	31.5
722B-40X-1	375.555	12.84	0.18	2.96	3.04	0.08		0.97	27.7	0.788	33.5	29.7	30.3	29.5	31.5
722B-40X-3	376.040	12.94	0.20	2.89	2.97	0.08		0.97	27.7	0.772	32.6	29.3	29.7	29.1	30.9
722B-41X-1	382.318	13.49	0.19	*2.17*	*3.12*	*0.96*	0.11	0.34	8.9	0.806	34.5	30.2	30.8	30.9	32.2
722B-41X-1-re	382.318	13.49	0.18	*2.15*	*3.09*	*0.93*				0.797	34.0	30.0	30.5	30.6	31.9
722B-41X-1	383.000	13.56	0.17	*2.83*	*3.28*	*0.45*				0.839	36.3	31.0	31.7	32.1	33.4

note

re: replicate analysis

Depth (mbsf): sampling depth (meters below sea floor).

The sampling interval is 3 centimeters (0.030 meters). The number shown in the 'Depth' column is the median number of sampling interval.

Table DR4. Sample information and TEX_{86}-SSTs and $U^{K'}_{37}$-SSTs at ODP Site 730A for the middle-late Miocene.

SAMPLE ID	Depth (mbsf)	AGE (Ma)	MI	RI	RI'	ΔR	BIT	Uk'37	SST	TEX86	Kim08	Liu09	Kim et al., 2010		
			Zhang et al., 2009	Zhang et al., 2016					Conte06				Liu09-revised	TEX86L	TEX86H
730A-4H-4	32.660	8.84	0.21	2.69	2.66	-0.03	0.01	0.97	27.6	0.696	28.3	27.0	27.0	24.0	27.8
730A-5H-5	43.138	9.13	0.18	2.78	2.71	-0.07	0.03			0.708	29.0	27.4	27.5	24.5	28.3
730A-7X-3	59.538	9.57	0.19	2.79	2.73	-0.07	0.02			0.713	29.3	27.6	27.7	25.7	28.5
730A-9X-1	76.404	10.01	0.33	2.40	2.69	0.29		0.95	27.0	0.703	28.7	27.2	27.3	25.0	28.1
730A-9X-5	81.753	10.09	0.26	2.44	2.54	0.10	0.05			0.663	26.5	25.8	25.7	24.0	26.4
730A-10X-1	86.053	10.16	0.22	2.66	2.68	0.02	0.03			0.701	28.6	27.2	27.3	25.7	28.1
730A-10X-5	91.953	10.25	0.22	2.66	2.69	0.03	0.02			0.704	28.8	27.3	27.4	25.5	28.2
730A-11X-4	99.835	10.37	0.23	2.72	2.80	0.08		0.96	27.3	0.730	30.2	28.1	28.3	26.4	29.2
730A-13X-4	119.083	10.71	0.19	2.83	2.90	0.07	0.03			0.754	31.6	28.8	29.2	27.5	30.2
730A-15X-4	138.288	11.05	0.19	2.91	2.97	0.07	0.02			0.772	32.6	29.3	29.7	29.2	30.9
730A-16X-4	147.643	11.22	0.18	2.86	2.93	0.07	0.02			0.763	32.1	29.1	29.5	27.9	30.6
730A-16X-4-re			0.18	2.86	2.94	0.08	0.03			0.763	32.1	29.1	29.5	28.0	30.6
730A-17X-4	160.945	11.46	0.20	2.77	2.92	0.15		0.96	27.4	0.760	31.9	29.0	29.4	27.7	30.4
730A-19X-2	174.168	11.77	0.19	2.86	2.98	0.12	0.03			0.774	32.7	29.4	29.8	29.3	31.0
730A-21X-3	194.417	12.26	0.19	2.73	2.96	0.23		0.96	27.5	0.768	32.4	29.2	29.6	27.9	30.8
730A-23X-4	215.178	12.77	0.18	2.85	3.02	0.17	0.06			0.783	33.2	29.6	30.1	29.2	31.3
730A-24X-3	224.149	12.99	0.18	2.81	3.01	0.20		0.94	26.6	0.780	33.1	29.5	30.0	28.5	31.2
730A-25X-6	237.968	13.30	0.18	2.95	3.12	0.16	0.08			0.804	34.4	30.2	30.7	30.2	32.1
730A-27X-4	254.215	13.66	0.18	2.85	3.08	0.22		0.96	27.3	0.795	33.9	29.9	30.5	29.5	31.8
730A-29X-1	269.203	13.98	0.18	2.85	3.13	0.28	0.07			0.807	34.5	30.2	30.8	31.0	32.2
730A-30X-5	284.575	14.32	0.19	2.89	3.11	0.22				0.802	34.3	30.1	30.7	31.0	32.1
730A-30X-5-re			0.19	2.86	3.10	0.23				0.800	34.2	30.1	30.6	31.0	32.0
730A-30X-CC	286.673	14.36	0.16	3.11	3.32	0.21	0.10			0.847	36.8	31.2	32.0	31.8	33.7
730A-31X-2	290.525	14.67	0.16	2.96	3.25	0.28		0.96	27.2	0.832	35.9	30.8	31.5	30.9	33.1
730A-31X-3	291.625	14.82	0.17	3.05	3.21	0.15		0.92	26.2	0.823	35.5	30.6	31.3	30.4	32.8

note

re: replicate analysis

Depth (mbsf): sampling depth (meters below sea floor).

The sampling interval is 3 centimeters (0.030 meters). The number shown in the 'Depth' column is the median number of sampling interval.